Chemical Engineering Journal 160 (2010) 538–548

Contents lists available at ScienceDirect

Chemical Engineering Journal

journal homepage: www.elsevier.com/locate/cej

Electrochemical oxidation of benzoic acid in water over boron-doped diamond electrodes: Statistical analysis of key operating parameters, kinetic modeling, reaction by-products and ecotoxicity

Theodora Velegraki[a], George Balayiannis[b], Evan Diamadopoulos[a], Alexandros Katsaounis[a], Dionissios Mantzavinos[a,*]

[a] Technical University of Crete, Department of Environmental Engineering, Polytechneioupolis, GR-73100 Chania, Greece
[b] Benaki Phytopathological Institute, Department of Pesticides Control and Phytopharmacy, GR-14561 Athens, Greece

ARTICLE INFO

Article history:
Received 6 October 2009
Received in revised form 24 March 2010
Accepted 25 March 2010

Keywords:
Benzoic acid
Boron-doped diamond
Electrochemical oxidation
Experimental design
Response surface methodology

ABSTRACT

The electrochemical oxidation of benzoic acid over boron-doped diamond electrodes was studied. Experiments were conducted in a flow-through electrolytic cell at current intensities ranging from 11 to 24 A, an electrolyte concentration of 0.05 M and initial substrate concentrations ranging from 16 to 185 mg L^{-1}. Liquid chromatography (LC) coupled to diode array detector was employed to follow benzoic acid concentration profiles, while chemical oxygen demand and dissolved organic carbon (DOC) analyses were carried out to assess the extent of mineralization. In preliminary experiments, the effect of different electrolytes ($NaNO_3$, NaCl or Na_2SO_4) and the initial pH of the solution (10 or 3.8) was evaluated. The effects of operating parameters such as applied current intensity, electrolysis time and initial benzoic acid concentration on the degradation and mineralization efficiency were investigated with the application of factorial design methodology and simple linear models describing and predicting adequately the removal of the substrate and DOC were developed. The initial substrate concentration and the treatment time constitute important parameters with regard to the efficiency of the process. Benzoic acid conversion proceeds through the hydroxylation of the aromatic ring as evidenced by the formation of several hydroxylated derivatives identified by LC coupled to mass spectroscopy (LC/MS-MS). Of these, monohydroxybenzoic acids appear to be quite stable to electrochemical oxidation. Toxicity tests with marine bacteria *V. fischeri* showed that, at the conditions in question, degradation by-products are consistently more toxic than the parent compound even after deep oxidation.

1. Introduction

Advanced oxidation processes involve the *in situ* generation of highly reactive chemical oxidants such as the hydroxyl radical ($OH^{\bullet}$) and have emerged as an important class of technologies for accelerating the oxidation of a wide range of organic contaminants to less harmful compounds and/or to their complete mineralization [1].

Electrochemical oxidation is a promising environmental remediation technology due to its effectiveness, easy operation and wide application. Electrochemistry makes the treatment of liquids, gases and solids possible, it is amenable to automation and compatible with the environment, because the main reagent, the electron, is a clean one [2], thus avoiding the use of strong oxidizing agents. In the context of wastewater treatment, electrochemical processes usually aim at either the conversion of biorecalcitrant organics to biocompatible organics or the combustion of organics which are completely oxidized to CO_2 [3].

In anodic oxidation [1,4–8] organic pollutants can be oxidized by highly oxidizing radical species formed on the high O_2-overvoltage anode surface through water oxidation:

$$H_2O \rightarrow OH_{ads}^{\bullet} + H^+ + e^- \quad (1)$$

Several anodes have been tested with some demonstrating selective oxidation (IrO_2) [9], while others either releasing toxic ions (PbO_2) or exhibiting limited service life (SnO_2) [10]. The use of a boron-doped diamond (BDD) thin film anode [11–14] in anodic oxidation has shown that its O_2-overvoltage is much higher than that of the aforementioned conventional anodes, thus producing larger amounts of adsorbed $OH^{\bullet}$ from water decomposition (reaction (1)), yielding faster destruction of pollutants [15]. The diamond surface is non-active in the sense that it does not provide any active sites for the adsorption of reactants and/or reaction by-products [6,16]. Therefore, hydroxyl radicals are considered to be the dominant

* Corresponding author. Tel.: +30 2821037797; fax: +30 2821037852.
E-mail address: mantzavi@mred.tuc.gr (D. Mantzavinos).

1385-8947/$ – see front matter © 2010 Elsevier B.V. All rights reserved.
doi:10.1016/j.cej.2010.03.065

species for the electrochemical combustion of organic pollutants; in addition, reactions of organic pollutants with oxygen species (e.g. H_2O_2 and O_3) and other electrochemically generated oxidants (e.g. in the presence of various electrolytes) are known to complement electrochemical activity [11,12,16–18].

Boron-doped diamond thin-films electrodes present some additional useful properties such as great chemical and electrochemical stability which enhance the average lifetime of this material and allow its use in the treatment of almost any kind of wastewater, high resistance to corrosion, high thermal stability, hardness and good electrical conductivity [19,20], thus being undoubtedly a promising material for the complete combustion of organics in wastewater treatment. The excellent properties of BDD anodes for electrochemical water treatment have been discussed thoroughly in a recent review article [16].

The goal of this work was to study the BDD electrochemical oxidation of benzoic acid (BA: C_6H_5COOH), a model compound representative of the aromatic fraction typically found in various industrial waste streams. BA also constitutes the parent molecule of several phenolic compounds such as vanillic, gallic, veratric, syringic, protocatechuic and hydroxybenzoic acids that are commonly found in agro-industrial effluents which are usually characterized by low biodegradability and high ecotoxicity [21]. Furthermore, BA is very commonly found in food and pharmaceutical products as antimicrobial preservative.

The effect of several operating parameters such as applied current, electrolysis time, initial BA concentration, the type of supporting electrolyte and initial solution pH on compound degradation and mineralization was investigated. An experimental factorial design methodology was adopted to elucidate the statistically important parameters, while the effect of the electrochemical oxidation of benzoic acid aqueous solutions on ecotoxicity was assessed.

To the best of our knowledge, information regarding the electrochemical degradation of BA is scarce in the literature. Montilla et al. [12] employed cyclic voltammetry and bulk electrolysis to study the electrochemical behavior of 257–1080 mg L^{-1} BA under galvanostatic conditions (1.5 A) on p-Si/BDD electrodes in perchloric acid solutions (0.5 M). They reported that electrolysis at high anodic potentials in the region of water and electrolyte decomposition led to the incineration of BA through complex oxidation reactions with hydroxyl radicals.

2. Experimental and analytical

2.1. Chemical reagents

Benzoic acid (99.5%), 4-hydroxybenzoic acid (99%) and cinnamic acid (99%) were provided by Fluka. Organic solvents utilized for HPLC analysis were provided by Riedel de Haén. Inorganic salts, namely Na_2SO_4 (99%, Riedel de Haén), NaCl (99%, Riedel de Haén) and $NaNO_3$ (99%, Fluka) were used as electrolytes. Working solutions were prepared daily by dissolving the appropriate amount of BA in deionized water at concentrations varying from 16 to 185 mg L^{-1}.

2.2. Electrolytic system

Experiments were conducted in a DiaCell (type 100) single compartment electrolytic flow-cell manufactured by Adamant Technologies (Switzerland). Two circular electrodes made of BDD on silicon were used as the anode and cathode; each electrode area was 70 cm^2 and the distance between them 0.01 m. Experiments were carried out in a recirculated batch mode under temperature control. A spiral coil immersed in the liquid and connected to tap water supply was used to remove the heat liberated from the reaction. The temperature increased during the first 15 min of reaction up to 28–35 °C, depending on the current intensity applied and remained constant thereafter. The working solution volume was 10 L for all experiments. A peristaltic pump was used to recirculate the solution through the electrochemical cell at a constant flow rate of 20 L min^{-1}. pH was left uncontrolled throughout the electrochemical treatment.

The cell potential was practically constant during the reaction, indicating that appreciable deterioration of the electrode and/or passivation phenomena did not take place [19]. The polarization changed automatically every 30 min, which helped to maintain the two electrodes free of intermediate product deposition on their surface.

2.3. Analytical methods

The degradation of benzoic acid was monitored by reversed-phase high performance liquid chromatography (HPLC) using a Shimadzu 10A*Vp* system comprising two LC-10AD*Vp* pumps, an autosampler (SIL-10AD*Vp*) and an SPD-M10A*Vp* diode array detector. Acidified water (pH of about 2.5) (solvent A) and acetonitrile (solvent B) were eluted through a C-18 column (4.6 mm × 250 mm; Prevail Organic Acid) under constant flowrate of 1 mL min^{-1}. The mobile phase followed a time program (0–5 min: B increases from 0% to 70% and A decreases from 100% to 30%; 5–10 min: B and A remain stable at 70% and 30%, respectively; 10–4 min: B decreases from 70% to 0% and A increases from 30% to 100%; 14–20 min: B and A remain stable at 0% and 100%, respectively). The injection volume was 20 μL and the temperature was kept constant at 30 °C. All samples were filtered (0.45 μm, Nylaflo, PALL) prior to analysis. HPLC was also employed to follow the concentration of 4-hydroxybenzoic and cinnamic acids during the respective electrochemical experiments.

Liquid chromatography coupled with tandem mass spectroscopy (LC/MS–MS) was employed to identify intermediate compounds accompanying BA degradation. A Varian HPLC system (Walnut Creek, CA, USA) comprising two pumps (Prostar 210), an autosampler (Prostar 420) with a 100 μl sample loop and column oven (Prostar 510) was employed. The chromatographic column was a Polaris 5u C18-A (2.1 mm × 150 mm, 5 μm particle size). The mobile phase, a mixture of methanol:water (5:95) at a flowrate of 0.2 mL min^{-1}, eluted isocratically. Each run lasted 15 min. All chromatographic solvents were degassed online with a vacuum degasser (Varian Prostar 590 Elite Micro Degasser). An electrospray ionization (ESI) interface (operated in the negative ion detection mode) was fitted to a Varian 1200 L triple quadrupole MS–MS system. Analysis was carried out under an argon pressure of approximately 2×10^{-6} atm in the collision cell.

The decay of dissolved organic carbon (DOC) during treatment was followed on a Shimadzu 5000A analyzer, whose operation is based on the combustion/non-dispersive infrared gas analysis. pH was determined with a Crison GLP 21 pH meter. Chemical oxygen demand (COD) reduction was determined colorimetrically according to the EPA approved reactor digestion method [22].

The luminescent marine bacteria *Vibrio fischeri* were used to assess the acute ecotoxicity of BA samples collected at fixed intervals during the process. The inhibition of *V. fischeri* was measured by the Microtox test system (Microtox 500 Analyzer (SDI, USA)) at exposure time of 15 min. The pH of the samples was adjusted to 7 ± 1 prior to toxicity tests with the addition of 0.1N HCl or 0.1N NaOH solutions, so that pH-related light inhibition was avoided. Furthermore, NaCl was added to the sample at 2% (w/v) concentration to exclude light inhibition due to osmotic phenomena.

2.4. Average oxidation state and partial oxidation efficiency

From the ratio between COD and DOC it is possible to calculate the value of the average oxidation state (AOS) of the organic carbon in solution as follows:

$$\mathrm{AOS} = \frac{4(\mathrm{DOC} - \mathrm{COD})}{\mathrm{DOC}} \quad (2)$$

with DOC and COD in molar concentrations.

AOS constitutes a potentially valuable parameter that can be used to estimate the degree of oxidation in a complex solution consisting of the initial compound and its oxidation by-products. It is based on the fact that the AOS of carbon can take values from −4 to +4.

However, its use does not provide information concerning the degree of partial and total oxidation that has occurred since the beginning of the reaction, but simply reports on the oxidation state at a given time without following the progress of partial oxidation reactions [23]. COD removal by partial oxidation ($\mathrm{COD_{partial}}$) at different reaction times can be expressed as follows [24]:

$$\mathrm{COD_{partial}} = \mathrm{COD_0}\left(\frac{\mathrm{DOC}}{\mathrm{DOC_0}}\right) - \mathrm{COD} \quad (3)$$

Eq. (3) can be expanded to give additional information with respect to the relative contribution of partial and total oxidation reactions that have occurred; the index ε represents the efficiency of COD removal through partial oxidation and is defined as the ratio of COD removal by partial oxidation to the overall COD removal [23]:

$$\varepsilon = \frac{\mathrm{COD_{partial}}}{(\mathrm{COD_0} - \mathrm{COD})} \quad (4)$$

where ε takes values from 0 to 1 corresponding to total and partial oxidation, respectively.

2.5. Instantaneous current efficiency

The data obtained from COD measurements during electrolysis were used for the determination of the instantaneous current efficiency (ICE) using the following equation [25,26]:

$$\mathrm{ICE}\ (\%) = 100\left[\frac{(\mathrm{COD}_t - \mathrm{COD}_{t+\Delta t})F\,V}{8\,I\,\Delta t}\right] \quad (5)$$

where COD_t and $\mathrm{COD}_{t+\Delta t}$ are the COD values (in $\mathrm{g\,O_2\,L^{-1}}$) at times t and $t+\Delta t$ (in s), respectively, I is the current intensity (A), F is the Faraday constant ($96487\ \mathrm{C\,mol^{-1}}$), V is the volume of the liquid (L) and 8 corresponds to a dimensional factor for unit consistency ($32\ \mathrm{g\,O_2\,mol^{-1}\ O_2}/4\ \mathrm{mol\,e^-\,mol^{-1}\ O_2}$).

2.6. Experimental factorial design methodology

Optimization of the treatment parameters of BA electrochemical oxidation was performed by experimental design and response surface methodology (RSM). This methodology was implemented employing the statistical software package MINITAB.

The first step in RSM is to determine a mathematical equation that describes the functional relationship between a response Y and a set of independent variables X. The mathematical expression of the response could be a first-order or second-order model that fits well in the region of the independent variables that is employed [27].

A central composite statistical design was used that comprises a 2^3 full factorial design, augmented by three center points and six star (axial) points. Three independent variables were converted to dimensionless ones (x_1, x_2, x_3), with values at five levels. The codified variables x_i are expressed as a function of their real values according to the following equation:

$$x_i = \frac{z_i - ((z_{+1} + z_{-1})/2)}{(z_{+1} - z_{-1})/2} \quad (6)$$

where z_i are the real (non-codified) values of variable x_i.

Table 1
Independent variables, their codified levels and actual values for the central composite design used in the present study.

Variable	Symbol	Real values of codified levels				
		$-a$	−1	0	+1	$+a$
Current intensity, I (A)	x_1	11.3	14	18	22	24.7
BA concentration, C_0 ($\mathrm{mg\,L^{-1}}$)	x_2	16	50	100	150	185
Treatment time, t (min)	x_3	99.5	120	150	180	200.5

The variables considered for this study were the applied current intensity (x_1), the initial concentration of the pollutant (x_2) and the treatment time (x_3). The selection of the variables and their levels (Table 1) was based on previous work [28] and preliminary experiments.

The axial points were selected at an $\alpha = (F)^{1/4} = \pm 1.68$ to assure the rotatability of the area of interest. The response factors were defined as: Y_1 = mass of benzoic acid removed per liter and Y_2 = mass of dissolved organic carbon removed per liter.

Regression analysis was applied in order to build an adequate model for each response factor and the goodness-of-fit and statistical significance of the models was assessed by analysis of variance (ANOVA) for 95% confidence interval.

3. Results and discussion

3.1. Screening experiments

To assess the effect of various electrolytes on the efficiency of the electrochemical oxidation of aqueous solutions of benzoic acid ($150\ \mathrm{mg\,L^{-1}}$), preliminary runs were performed at 14 A, in the presence of 0.05 M $NaNO_3$, NaCl or Na_2SO_4. The effect of solution pH was also investigated by treating BA solutions of $150\ \mathrm{mg\,L^{-1}}$ concentration at 18 A, in the presence of 0.05 M Na_2SO_4 and at initial pH values of 3.8 and 10. Table 2 summarizes the results obtained from the aforementioned experiments. It is shown that Na_2SO_4 results in the highest BA conversion (35%) after 2 h of electrochemical treatment, compared to $NaNO_3$ and NaCl, that yield 23% and 15% conversion, respectively. Thus, after 2 h of treatment the concentration of BA removed is $46\ \mathrm{mg\,L^{-1}}$ with Na_2SO_4, $32\ \mathrm{mg\,L^{-1}}$ with $NaNO_3$ and just $19\ \mathrm{mg\,L^{-1}}$ with NaCl. The superiority of Na_2SO_4 compared to the other two salts may be associated with the generation of peroxodisulfate [17] (Eq. (7)), a powerful oxidizing agent that can enhance the hydroxyl radical-induced degradation of BA.

$$2SO_4^{2-} \rightarrow S_2O_8^{2-} + 2e^- \quad (7)$$

After 1 and 2 h of treatment at 18 A, BA removal at inherent pH (3.8) reached 25% and 41%, respectively, which is about twice as much as that achieved at alkaline conditions. In this view, all subsequent runs were conducted at the solution's inherent pH.

Fig. 1 shows the evolution profiles of normalized DOC and BA concentrations with the electrical charge passed, during the electrochemical oxidation of $50\ \mathrm{mg\,L^{-1}}$ benzoic acid at 14 A in the presence of 0.05 M Na_2SO_4. It is demonstrated that DOC is satisfactorily diminished and the formation of carbon dioxide commences from the initial stages of the treatment. After 2 h of treatment, 56% removal of BA is achieved, which is 20% higher than the respective removal accomplished for $150\ \mathrm{mg\,L^{-1}}$ BA under similar experimental conditions (Table 2). Almost complete removal of the initial compound can be achieved after the consumption of $9.8\ \mathrm{Ah\,L^{-1}}$

Table 2
Effect of the type of electrolyte (0.05 M) and initial pH on BA (150 mg L^{-1}) conversion at different current intensities and reaction times. ND, not determined.

Time (min)	Current intensity (A)	Type of Electrolyte	Initial pH	Conversion (%)	BA removed (mg L^{-1})
30	14	NaCl	3.8	7	9
120				15	19
30		$NaNO_3$		ND	ND
120				23	32
30		Na_2SO_4		15	20
120				35	46
30	18	Na_2SO_4	3.8	14	22
60				25	39
120				41	64
30			10	ND	ND
60				10	13
120				22	29

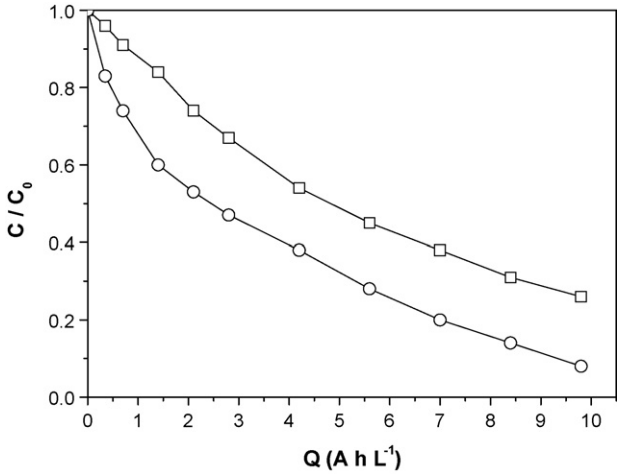

Fig. 1. DOC (□) and benzoic acid (○) abatement as a function of the applied charge passed. Operating conditions: 14 A; T = 28 °C; Na_2SO_4 0.05 M; BA 50 mg L^{-1}; inherent pH.

(7 h). The remaining DOC (9 mg L^{-1}) can be attributed to oxidizable degradation by-products still present after the end of the treatment. As will be discussed in following sections, LC/MS–MS analysis confirmed the presence in the reaction mixture of various hydroxylated benzoic acid derivatives.

Fig. 2 shows the progress of AOS and the efficiency of partial oxidation ε with time for different benzoic acid concentrations at 18 A and 0.05 M Na_2SO_4. The initial AOS value of the aqueous solutions of benzoic acid varies from −0.4 to −0.2. If the oxidation of BA and its degradation by-products to CO_2 was complete and occurred rapidly, the AOS would remain nearly unchanged during electrolysis. However, the AOS increases gradually throughout the reaction and this indicates that more oxidized molecular structures are formed during treatment. As can be seen, the increase of AOS is more pronounced at lower BA concentrations. The AOS increases from −0.4 to about 1 (i.e. 1.4 units increase) at 16 mg L^{-1}, from −0.2 to 0.6 (i.e. 0.8 units increase) at 100 mg L^{-1} and from −0.4 to 0.08 (i.e. 0.48 units increase) at 185 mg L^{-1} initial BA concentration, respectively. This means that more oxidized intermediates are formed during treatment of lower initial concentrations of BA.

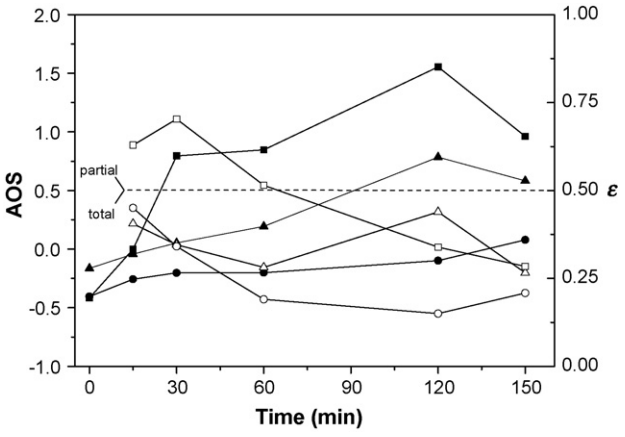

Fig. 2. Changes in the average oxidation state, AOS (closed symbols) and in the efficiency of COD removal by partial oxidation, ε (open symbols) at different initial concentrations of BA: (□, ■) 16 mg L^{-1}; (▲, Δ) 100 mg L^{-1}; (●, ○) 184 mg L^{-1}. Operating conditions: 18 A; T = 31 °C; Na_2SO_4 0.05 M; inherent pH.

Total oxidation seems to be dominant since ε is, in most cases, lower than 0.5 (i.e. more than 50% of the overall COD removal is due to total oxidation reactions). This threshold value is represented in Fig. 2 by a dashed line, above which the COD removal achieved is mainly due to partial oxidation reactions, while below it is mainly attributed to total oxidation reactions.

Fig. 3a–c depict the concentration of BA, COD and DOC removed, respectively as a function of charge passed during the electrochemical oxidation of 100 mg L^{-1} BA. It is observed that the concentration of BA and DOC removed remains practically unaffected by the applied current intensity, which means that the same efficiency (in terms of mass removed) can be attained at either longer treatment times and lower current intensities or, conversely, at shorter treatment times and higher current intensities. However, the mass of COD removed seems to increase slightly at lower current intensities (Fig. 3b). For example, the mass of COD removed is 49 mg L^{-1} at 24.7 A and 67 mg L^{-1} at 11.3 A after about 2.5 Ah L^{-1} of charge passed. In other words, to remove the same amount of COD, e.g. 73 mg L^{-1}, would require 3.7Ah L^{-1} (or 90 min of treatment) at 24.7 A and 2.8 Ah L^{-1} (or 150 min of treatment) at 11.3 A. This may be due to the fact that part of the electrogenerated radicals are wasted to side reactions such as O_2 evolution (Eq. (8)) and this phenomenon is more pronounced at higher current intensities; this behavior is characteristic of mass transfer controlled processes in which an increase in the current density cannot enhance the rate of oxidation of the organics at the electrode but favors anodic side reactions [29].

$$H_2O \rightarrow 1/2O_2 + 2H^+ + 2e^-. \quad (8)$$

Side reactions on the anode surface act competitively against the indirect degradation of the organics [5], whereas at lower current intensities the majority of $HO^\bullet$ radicals are utilized for the degradation of the organic compounds.

Interestingly, the effect of applied current intensity on the extent of COD removal (for the same charge) was not observed in the case of DOC removal (Fig. 3c) although both COD and DOC are gross, lumped parameters of the liquid phase organic content. It should be taken into account that changes in COD are related to a complex reaction network that includes chemical transformations

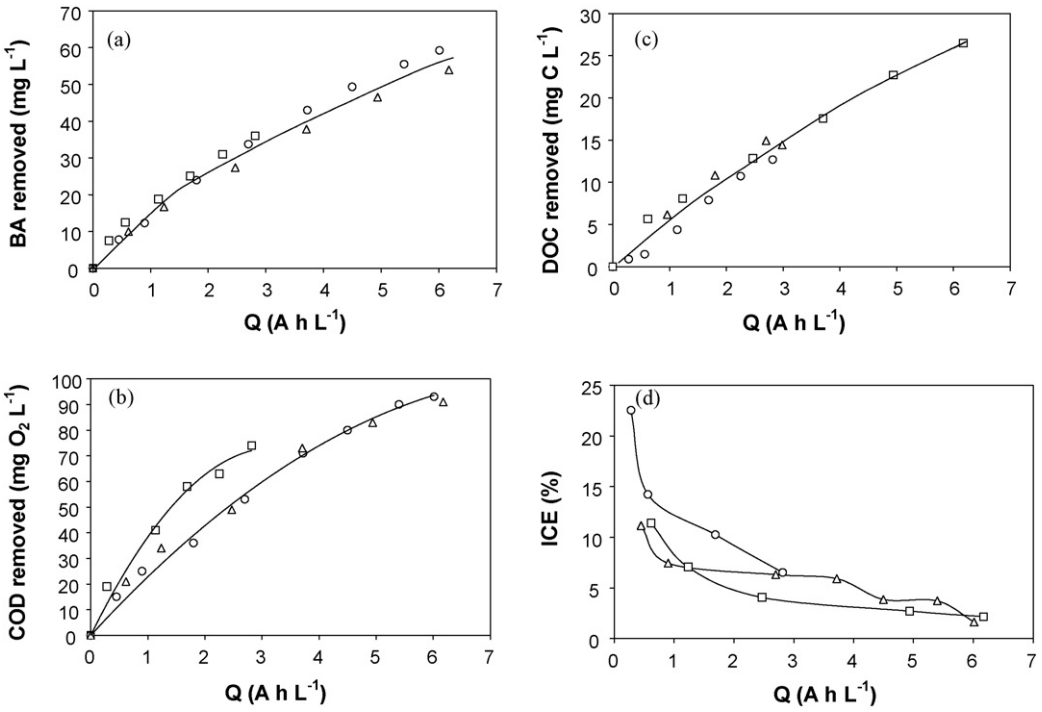

Fig. 3. Effect of current intensity at (□) 11.3 A; (○) 18 A; (△) 24.7 A on 100 mg L^{-1} BA oxidation. Variation of concentration of (a) BA removed; (b) COD removed; (c) DOC removed; (d) ICE, with reference to applied charge passed. Operating conditions: Na_2SO_4 0.05 M; T = 26–31 °C; inherent pH.

such as dimerization, polymerization, partial and total oxidation. On the contrary, changes in DOC are solely related to the complete oxidation of liquid phase organic carbon to CO_2 without taking into account other chemical transformations. It can be hypothesized that total oxidation reactions are less susceptible to changes in the applied current (for the same charge) than partial oxidation and possibly other reactions and this would explain the different behavior of COD and DOC.

At the experimental conditions in question, ICE is not affected significantly by variations in the applied current intensity (Fig. 3d). The relatively low ICE values recorded indicate that oxidation proceeds under current intensities considerably greater than those stoichiometrically required to oxidize the organic content present in the solution. These results are typical for the electrochemical treatment of solutions with low COD content [14,30,31] and are attributed to mass transfer limitations of the organic compounds to the anode surface. The higher ICE values (i.e. 22% at 18 A) observed at the early stages of the reaction are due to the higher concentrations of BA and other intermediates initially available to react. As the reaction proceeds, the efficiency drops continuously and this is probably associated with the progressive formation of intermediates, such as short carboxylic acids, that are more resistant to electrochemical oxidation.

The aforementioned screening runs clearly highlight the potentially important effects of initial BA concentration, electrolysis time and current intensity on the performance of the electrochemical process; in this respect, these parameters are investigated further in a more systematic way.

3.2. Statistical analysis

Table 3 shows the central composite design matrix, the combinations of the independent variables x_1, x_2 and x_3 and the corresponding experimental values of responses Y_1 and Y_2 (mass of BA and DOC removed per liter, respectively). The experiment at the center of the design was carried out three times (runs 9, 10 and 11 in Table 3) in order to obtain an estimation of the experimental standard error [28,32].

Table 4 shows all model parameters, in terms of statistical significance, that affect responses Y_1 and Y_2. Only terms that were found statistically significant ($p < 0.05$) were included in the reduced models that are discussed later [33]. It is depicted that the initial concentration of BA (x_2) is an important factor for both response variables. Moreover, electrolysis time (x_3) is very close to the threshold p-value of 0.05, therefore, it was included in the reduced model describing Y_1.

One way to assess the significance of the effects and the existence of curvature in the system is to perform repeat runs at the center point of the design (i.e. the variables receive mean values between their high and low levels) and make an estimation of the

Table 3
Central composite statistical design matrix showing the combinations of experimental conditions and the respective responses Y_1 and Y_2. ND, not determined.

Run	Type	x_1	x_2	x_3	Y_1	Y_2
1	*Full design*	−	+	−	52	40
2		+	+	+	85	ND
3		−	+	+	75	34
4		−	−	+	44	18
5		+	−	+	52	21
6		+	−	−	43	16
7		−	−	−	32	10
8		+	+	−	70	26
9	*Center runs*	0	0	0	57	24
10		0	0	0	53	25
11		0	0	0	54	26
12	*Axial or star*	0	0	$-a$	36	14
13	*points*	$-a$	0	0	36	13
14		0	$+a$	0	50	35
15		0	0	$+a$	59	28
16		$+a$	0	0	54	26
17		0	$-a$	0	11	5

Table 4
Statistical significance of parameters of full quadratic models with regard to responses Y_1 and Y_2.

Parameter	Mass of BA removed per liter (Y_1)		Mass of DOC removed per liter (Y_2)	
	Estimate	p-Value	Estimate	p-Value
Intercept	53.61	0.000*	24.7	0.000*
x_1	5.65	0.107	0.97	0.592
x_2	12.93	0.004*	8.48	0.003*
x_3	7.15	0.052*	2.55	0.187
x_1x_2	1.12	0.786	−3.32	0.213
x_2x_3	2.12	0.611	−1.82	0.473
x_1x_3	−1.37	0.741	0.92	0.712
$(x_1)^2$	0.23	0.947	−0.93	0.609
$(x_2)^2$	−4.89	0.189	−0.75	0.677
$(x_3)^2$	1.11	0.750	−0.40	0.823

* Statistically significant at $\alpha = 0.05$.

standard error according to Eq. (9):

$$\text{MSPE} = \sum \frac{(Y_i - Y_m)^2}{(\text{total number of repeat runs} - 1)} \quad (9)$$

where Y_i is the response of the ith repeat run and Y_m is the mean value of the repeated responses. Standard error for each model was calculated at a value of 2.08 (response Y_1) and at a value of 1 (response Y_2) according to Eq. (9). If an effect is about or below the standard error, it may be considered insignificant (or in other terms, not different from zero). Pareto charts (Fig. 4) help to identify the most influential factors through a comparison of the relative magnitude of the effects and an evaluation of their statistical significance. Fig. 4 displays the absolute value of the effects and the reference line ($t_{Res.dof, 0.025}$) that is computed by the error terms and corresponds to $\alpha = 0.05$. Any effect that extends past the reference line is potentially important. Therefore, the effect of initial pollutant concentration (x_2) seems to have a significant positive effect on Y_1 (Fig. 4a), while electrolysis time (x_3), since it marginally reaches the reference line and its effect is not evaluated clearly, is worth investigating further and is also added to the reduced model. Likewise, initial pollutant concentration (x_2) is found to have the most significant positive effect on Y_2 (Fig. 4b). No curvature was detected in the system, for the experimental area under investigation, which implies that a full complex model with all parameters is unnecessary. The system is characterized by linearity and can, therefore, be described adequately by simpler linear models.

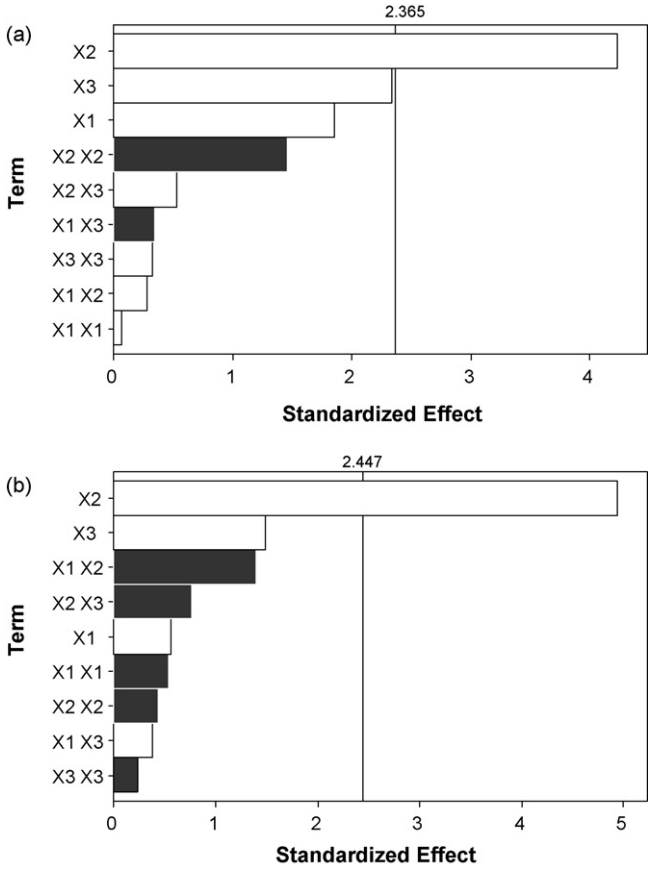

Fig. 4. Pareto charts indicating the statistically important effects of main, interaction and quadratic terms for response variables: (a) Y_1; (b) Y_2. White bars: positive effect; Black bars: negative effect.

Table 5
ANOVA for the reduced models of Eqs. (10) and (11).

Source	DF	SS	MS	F	p
$Y_1 = 50.8 + 12.9x_2 + 7.2x_3$					
Regression	2	2982	1491	11.9	0.001
Residual error	14	1759	125.6		
Lack of fit	6	1171.7	195.3	2.7	0.101
Pure error	8	587.3	73.4		
Total	16	4741.1			
$Y_2 = 23.3 + 8.8x_2 + 2.9x_3$					
Regression	2	1031.3	515.7	20.4	0.000
Residual error	13	328.6	25.3		
Lack of fit	6	85.3	14.2	0.4	0.852
Pure error	7	243.3	34.8		
Total	15	1359.9			

As a result, all the interaction and quadratic terms, as well as the main effect of current intensity (Table 4) were dropped and new reduced linear models (Eqs. (10) and (11)) were developed. To assess the goodness-of-fit of the reduced models, ANOVA was performed for the second time (Table 5).

$$Y_1 = 50.8 + 12.9x_2 + 7.2x_3 \quad (10)$$

$$Y_2 = 23.3 + 8.8x_2 + 2.9x_3 \quad (11)$$

The p-values (0.001 and 0.000) in the ANOVA tables show that the reduced models estimated by the regression procedure are significant at an α-level of 0.05. The p-values of the estimated coefficients of x_2 and x_3 for the first model are 0.001 and 0.033, respectively (data not shown), indicating that they are significantly related to the response Y_1. Likewise, the p-values for the second model are equal to zero (data not shown) which also confirms the significance of these parameters concerning the response Y_2. Both models demonstrated good fit and were found significant by the F-test at the 5% confidence level (Prob > F < 0.05) [34]. Analysis of variance for both models was also performed and statistical parameters were obtained (data not shown for brevity), indicating that the reduced models fit the data satisfactorily.

The diagnostic plots (Fig. 5) verify that the assumptions of normality, independence and randomness of the residuals (i.e. the difference between the observed and predicted or fitted values of each response) are satisfied. From the normal probability plots of the residuals for the two reduced models, it can be seen that the residuals follow the fitted line fairly closely; this confirms that (i) the residuals follow normal distribution with mean value close to zero, and (ii) the effects that were assumed insignificant during the development of the reduced models can be readily explained as random noise. The estimated p-values for each Anderson–Darling goodness-of-fit test are greater than 0.05, suggesting that the data follow a normal distribution.

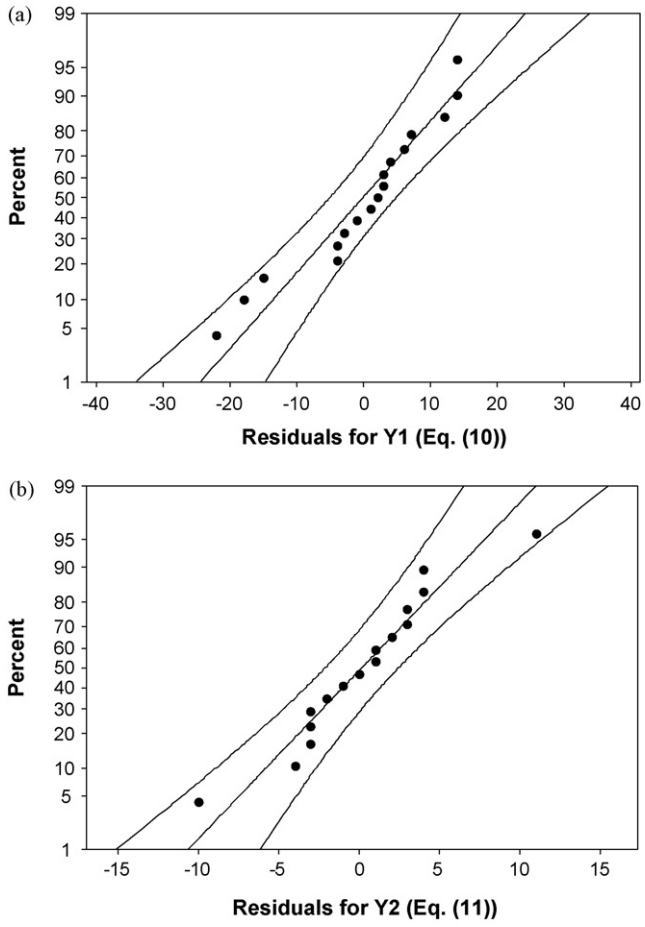

Fig. 5. Normal probability plot of the residuals for (a) Y_1; (b) Y_2.

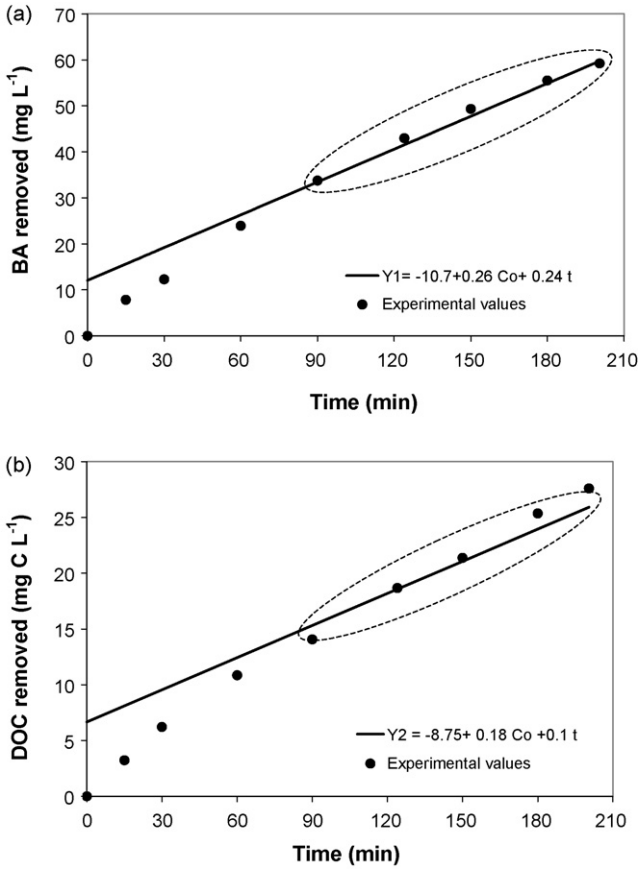

Fig. 6. Comparison between experimental and predicted values with respect to the concentration of (a) BA (Eq. (12)); (b) DOC (Eq. (13)) removed. Operating conditions as in Run 15, Table 3: 18 A; T = 27 °C; Na_2SO_4 0.05 M; BA 100 mg L^{-1}; inherent pH.

Taking into consideration the reduced linear models of Eqs. (10) and (11), an attempt was made to evaluate the goodness-of-fit of the computed data (i.e. derived from the model) with the observed data (i.e. derived from the experiments). In order to do this, the codified forms of the independent variables x_2 and x_3 are transformed to their corresponding non-codified forms through Eq. (6) and the resulting expressions of the response variables Y_1 and Y_2 are:

$$Y_1 = -10.7 + 0.26\,C_0 + 0.24\,t \quad (12)$$

$$Y_2 = -8.75 + 0.18\,C_0 + 0.1\,t \quad (13)$$

where C_0 (mg L^{-1}) and t (min) are the initial BA concentration and electrolysis time, respectively.

Representative data are shown in Fig. 6 where the experimental values of Run 15 in Table 3 are compared to the respective values derived from Eqs. (12) and (13). For a given value of x_1 (i.e. 18 A) and x_2 (i.e. 100 mg L^{-1}), both models fit well throughout the whole range of x_3 studied (i.e. from 99 to 200 min shown by the marked area). At lower treatment times, the discrepancy between experimental and predicted values becomes expectedly pronounced, thus implying that the models may be inadequate for predictions outside the range of conditions for which they were developed.

3.3. Modeling of COD evolution and comparison with experimental data

The electrochemical oxidation of 50 mg L^{-1} BA at 14 A results in an exponential decrease of COD with time, as clearly seen in Fig. 7a. This trend is typical of a mass transport-controlled process [17,31,35], during which oxidation is controlled by the rate at which organic molecules are carried from the liquid bulk to the electrode surface rather than by the rate at which electrons are delivered to the anode.

In previous studies [17,35], a theoretical model capable of predicting temporal COD evolution during the electrochemical oxidation of organic compounds on BDD thin electrodes was developed. At conditions of mass transport control ($j > j^0_{lim}$), the model is expressed as follows:

$$\mathrm{COD}_t = \beta\,\mathrm{COD}_0 \exp\left(-A\frac{k_m}{V}t + \frac{1-\beta}{\beta}\right) \quad (14)$$

where COD_0 and COD_t are the initial and at time t (in s) COD (in mol O_2 m^{-3}), A is the electrode area (m^2), k_m is the mass transfer coefficient in the electrochemical reactor (m s^{-1}), V is the liquid volume (m^3), $\beta = j/j^0_{lim}$, and j and j^0_{lim} are the applied and initial limiting current density (A m^{-2}), respectively.

At the experimental conditions under consideration, $j \gg j^0_{lim}$ and β becomes equal to unity, thus reducing Eq. (14) to:

$$\mathrm{COD}_t = \mathrm{COD}_0 \exp\left(-A\frac{k_m}{V}t\right) \quad (15)$$

In a recent work of our group [36], the mass transfer coefficient was determined equal to 1.75×10^{-5} m s^{-1} for the electrochemical reactor in question using the ferri/ferrocyanide redox couple and the limiting current density values. If this k_m value is taken into account, the model clearly underestimates the oxidation capacity of the electrochemical process (dashed line in Fig. 7a) since the COD decrease is always greater than the theoretical one. As a matter of fact, regression of the experimental data (solid line in Fig. 7a) yields a mass transfer coefficient that is about 5 times greater than

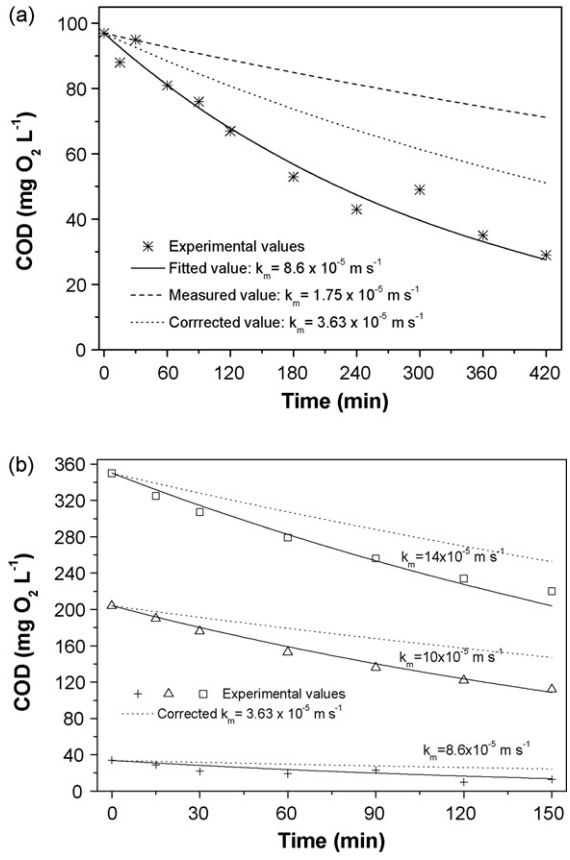

Fig. 7. Comparison between experimental and predicted COD profiles during the electrochemical oxidation of (a) 50 mg L^{-1} BA at 14 A; (b) different BA concentrations, i.e. (+) 16 mg L^{-1}; (Δ) 100 mg L^{-1}; (□) 184 mg L^{-1} at 18 A. Solid, dashed and dotted lines represent model prediction with the fitted, measured and corrected k_m values, respectively. Operating conditions: Na_2SO_4 0.05 M; T = 28–31 °C; inherent pH.

the measured one. The discrepancy between experimental and predicted values may be due to the following reasons: firstly, the model only takes into account the HO•-induced reactions near the anode surface, while the contribution of oxidation reactions driven by various electrogenerated species in the liquid bulk (e.g. peroxodisulfate) is completely disregarded [17]. Secondly, the fast redox reaction of the ferri/ferro couple employed to determine k_m does not consider the different organic species (i.e. BA and its degradation by-products) and reactions occurring in the system under consideration. In an attempt to correct the k_m value to take into account the presence of a specific organic or mixture of organics, the following procedure is suggested:

The mass transfer coefficient for benzoic acid oxidation, $k_{m_{BA}}$ is given as follows:

$$k_{m_{BA}} = \frac{D_{BA}}{\delta} \quad (16)$$

where D_{BA} is the diffusion coefficient of benzoic acid (0.95×10^{-9} m^2 s^{-1} [37]) and δ is the thickness of the diffusion layer (m). Assuming that δ is common for both the ferri/ferrocyanide and benzoic acid systems, it can be determined from Eq. (16) provided that the diffusion coefficient of the ferri/ferro couple, D_{FF} is known.

Application of the above methodology directly to our system was not possible due to the fact that the electrochemical reactor consists of identical anode and cathode electrodes. Therefore, the procedure was applied to another electrochemical reactor [38] consisting of BDD and zirconium as the anode and cathode, respectively. D_{FF} was determined equal to 0.45×10^{-9} m^2 s^{-1}

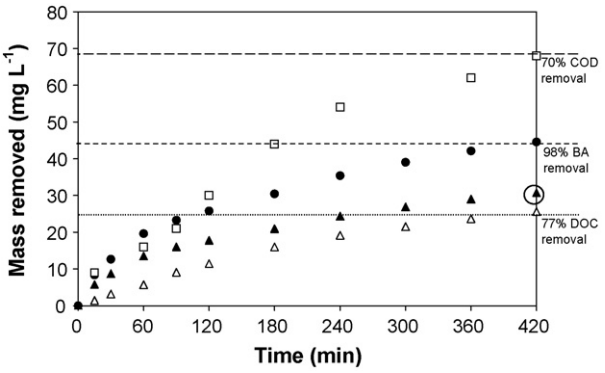

Fig. 8. Changes in the concentration of (●) BA; (Δ) DOC; (▲) carbon contained in BA; (□) COD removed with electrolysis time. Operating conditions: 14 A; T = 28 °C; Na_2SO_4 0.05 M; BA 50 mg L^{-1}; inherent pH.

using linear sweep voltammetry as described in detail elsewhere [39] and δ was computed equal to 2.6×10^{-5} m. Based on this δ value, $k_{m_{BA}}$ becomes 3.63×10^{-5} m s^{-1}, i.e. twice as much as that of the ferri/ferro couple. Fig. 7a and b shows predicted COD profiles based on the corrected mass transfer coefficient (dotted lines) and, despite the better fitting, there is still a significant deviation from the experimental data and the respective fitted mass transfer coefficients. Although this deviation may, to some degree, be associated with the complexity of the reaction system in question (i.e. involving various by-products, mechanisms and kinetics), it can safely be hypothesized that reactions in the liquid bulk play an important role in the pathways leading to the destruction of BA and its degradation by-products.

3.4. Determination and reactivity of intermediates

Fig. 8 shows temporal profiles of the concentrations of BA, COD and DOC removed during the electrochemical treatment of 50 mg L^{-1} BA for 7 h at 14 A. BA is rapidly oxidized and nearly complete removal can be achieved after 7 h, while the respective extent of COD and DOC removal is 70% and 77% which implies the presence in the reaction mixture of intermediates that are more resistant to electrochemical oxidation than the parent compound.

Fig. 8 also shows the temporal profile of theoretical DOC removed if all BA were immediately converted to CO_2, i.e. no stable intermediates remained in the liquid phase. For example, the point encircled in Fig. 8 represents the theoretical amount of DOC removed (32 mg L^{-1}) upon the almost complete oxidation of BA and this value corresponds to the measured DOC of the initial 50 mg L^{-1} BA solution. The discrepancy between measured and theoretical DOC values shown in Fig. 8 (open and closed triangles) corresponds to the presence of liquid phase organic intermediates accompanying the degradation of BA.

The LC/MS–MS analysis revealed the formation of several hydroxylated intermediate compounds, namely hydroxybenzoic acid(s) (HBAs), dihydroxybenzoic acid(s) (DHBAs) and trihydroxybenzoic acid(s) (THBAs). HBAs are formed from the early stages of the reaction and are still present after prolonged treatment, signifying a rather stable chemical structure and/or a production rate that is greater than their destruction rate. On the contrary, DHBAs and particularly THBAs seem to be readily oxidized. A comparison of the peak areas of the intermediates with the peak area of the parent compound reveals that HBAs are the most abundant intermediates followed by DHBAs, whereas THBAs are only present at trace quantities. The present findings are in agreement with a recent work [40] regarding the BDD electrochemical oxidation of 3,4,5-THBA (i.e. gallic acid) which is readily mineralized through the formation of aliphatic intermediates. LC/MS–MS also verified

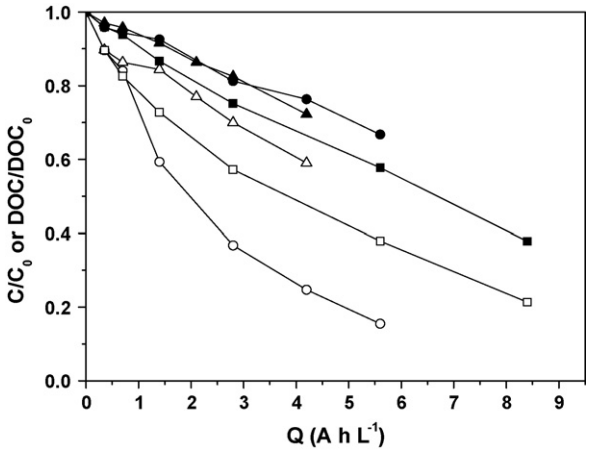

Fig. 9. Abatement of (■, □) BA; (▲, △) 4-HBA; (●, ○) CA as a function of the applied charge passed. Open symbols refer to specific compound and closed symbols to DOC. Operating conditions: 14 A; T = 28 °C; Na_2SO_4 0.05 M; BA or 4-HBA or CA 50 mg L^{-1}; inherent pH.

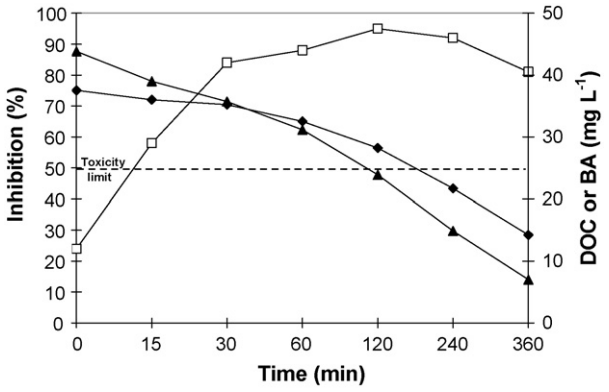

Fig. 10. Changes in (□) toxicity and in the concentration of (▲) BA; (♦) DOC with electrolysis time. Operating conditions: 14 A; T = 26 °C; Na_2SO_4 0.05 M; BA 50 mg L^{-1}; inherent pH.

the abatement of BA during the electrochemical process. It should be pointed out here that other ring or ring-cleavage intermediates could not be positively determined with the analytical equipments and protocols employed in this study. From these findings, it can be inferred that the hydroxylation of the aromatic ring is an important pathway during the early stages of BA electrochemical oxidation; this path has already been suggested for the TiO_2-induced photocatalytic degradation [41] and photo-Fenton oxidation [42] of the same compound. Montilla et al. [12] reported the formation of 2-HBA, 2,5-DHBA and hydroquinone during the BDD electrochemical oxidation of BA, without providing though additional information concerning their abundance or at which point of the treatment they appear.

It was then decided to investigate the reactivity of 4-HBA, member of the HBAs family of reaction intermediates that accompany the electrochemical oxidation of BA. Although chemistry laws dictate that electrophilic aromatic substitution is most likely to occur at the meta- rather than the ortho- or para-position [43], 4-HBA was chosen over its ortho- and meta-isomers because in previous studies dealing with the advanced oxidation of benzoic acid [41,42], it was detected at slightly higher concentrations than its isomers. (It should be noted that LC/MS–MS analysis is not capable of discriminating amongst the various hydroxylated isomers.)

Fig. 9 shows the evolution profiles of normalized DOC and 4-HBA concentrations with the electrical charge passed, during the electrochemical oxidation of 50 mg L^{-1} 4-HBA at 14 A. To allow for an easy comparison, data from an identical run with BA are also given. As seen, 4-HBA is less susceptible to electrochemical oxidation than its parent compound. For instance, 4-HBA conversion after 2.8 Ah L^{-1} of charge passed is 30%, while the respective value for BA is 43%. In a previous study dealing with the photo-Fenton oxidation of BA and its derivatives [42], 4-HBA was found to be more readily oxidizable than BA and this was attributed to the role of the attached hydroxyl group facilitating the electrophilic attack by HO(in the liquid bulk [44,45]. Taking into account that photo-Fenton and BDD electrochemical oxidation occur, to a certain degree, through different reaction mechanisms, this would explain the discrepancies in the observed reactivities. It can be speculated that BA and 4-HBA exhibit different affinity to reactions with hydroxyl radicals on the anode surface and/or with peroxodisulfate in the liquid bulk [46,47]. Fig. 9 also shows that the extent of 4-HBA degradation is expectedly lower than its mineralization, thus implying the presence of reaction by-products; LC/MS–MS analysis confirmed the formation of DHBAs and THBAs and their existence is consistent with the hydroxylation of the aromatic ring, a pathway already observed with BA as the starting molecule.

In a final run, the reactivity of cinnamic acid (CA) was tested and results are also shown in Fig. 9. Like BA, CA (C_6H_5CH=$CHCOOH$) constitutes the parent molecule of several (mainly hydroxylated) derivatives typically found in various industrial effluents. As seen, CA exhibits substantially higher reactivity than BA and this is owing to the exocyclic double bond that makes the molecule more susceptible to oxidative attack. Again, hydroxylation of the aromatic ring occurs as evidenced by the formation of coumaric and caffeic acids (mono- and dihydroxylated derivatives, respectively), as well as ferulic acid (a monohydroxylated derivative also bearing a methoxy group).

3.5. Evaluation of ecotoxicity

Fig. 10 shows changes in toxicity (expressed as percent inhibition of bioluminescence) to sea bacteria *V. fischeri*, as well as in BA and DOC concentrations as a function of treatment time during the electrolysis of 50 mg L^{-1} BA at 14 A. Although the original solution is only partially toxic (23% inhibition) to the test microorganism, toxicity increases sharply during the early stages of the reaction (e.g. 80% inhibition after 30 min) and remains high throughout the course of the treatment. This clearly implies that degradation by-products are considerably more toxic than the parent compound; even after 6 h of reaction where 60% of the carbon initially present in the reaction mixture has been converted to CO_2, inhibition is as high as 80%, indicating the toxic nature of the liquid phase by-products that account for about two thirds of the residual DOC. Similar results regarding the toxicity of the parent compound and its reaction intermediates were reported for the heterogeneous photocatalytic degradation of benzoic acid [41].

4. Conclusions

This study dealt with various aspects of the electrochemical oxidation of benzoic acid, a model aromatic pollutant, over boron-doped diamond electrodes. The following conclusions can be drawn:

(1) Several factors may be decisive for the successful operation of the process. To evaluate in a coherent way the importance of the various parameters involved, response surface methodology and regression analysis were implemented. Both

the initial concentration of the pollutant and the treatment time constitute important parameters that influence treatment efficiency.

(2) Simple linear models were developed which adequately simulated quantitatively the amount of benzoic acid and DOC removed as a function of the most significant main effects. The development of such empirical models with relatively few experiments is of great importance as they can form the basis for process optimization and scale-up. It should be noticed though that such models can work satisfactorily within the range of conditions from which they have been developed and may be viewed with caution at conditions outside this range.

(3) The reaction pathways of benzoic acid electrochemical abatement involve (i) the attack of the aromatic ring by hydroxyl radicals, as evidenced by the formation of several hydroxylated derivatives, and (ii) total oxidation reactions that dominate over partial oxidation, thus explaining the fast mineralization of intermediates to carbon dioxide. Although the primary reaction zone is believed to be near the BDD surface, reactions in the liquid bulk stimulated by e.g. peroxodisulfate (which is associated with the use of Na_2SO_4 as the supporting electrolyte) and/or other electrogenerated species cannot be excluded.

(4) Reaction by-products exhibit different reactivities to electrochemical oxidation and this is attributed to differences in chemical structures. Furthermore, by-products are more toxic to marine bacteria than benzoic acid.

Acknowledgments

This work is part of the 03ED375 research project, implemented within the framework of the "Reinforcement Program of Human Research Manpower" (PENED) and co-financed by National and Community Funds (75% from EU-European Social Fund and 25% from the Hellenic Ministry of Development-General Secretariat of Research and Technology).

References

[1] B. Nasr, T. Hsen, G. Abdellatif, Electrochemical treatment of aqueous wastes containing pyrogallol by BDD-anodic oxidation, J. Environ. Manage. 90 (2009) 523–530.
[2] K. Juttner, U. Galla, H. Schmieder, Electrochemical approaches to environmental problems in the process industry, Electrochim. Acta 45 (2000) 2575–2594.
[3] G. Chen, Electrochemical technologies in wastewater treatment, Sep. Purif. Technol. 38 (2004) 11–41.
[4] A. Ozcan, Y. Sahin, A.S. Koparal, M.A. Oturan, Propham mineralization in aqueous medium by anodic oxidation using boron-doped diamond anode: influence of experimental parameters on degradation kinetics and mineralization efficiency, Water Res. 42 (2008) 2889–2898.
[5] M. Murugananthan, S. Yoshihara, T. Rakumab, T. Shirakashi, Mineralization of bisphenol A (BPA) by anodic oxidation with boron-doped diamond (BDD) electrode, J. Hazard. Mater. 154 (2007) 213–220.
[6] A.M. Faouzi, B. Nasr, G. Abdellatif, Electrochemical degradation of anthraquinone dye Alizarin Red S by anodic oxidation on boron-doped diamond, Dyes Pigments 73 (2007) 36–39.
[7] D. Montanaro, E. Petrucci, Electrochemical treatment of Remazol Brilliant Blue on a boron-doped diamond electrode, Chem. Eng. J. 153 (2009) 138–144.
[8] N. Bensalah, M.A. Quiroz Alfaro, C.A. Martinez-Huitle, Electrochemical treatment of synthetic wastewaters containing Alphazurine A dye, Chem. Eng. J. 149 (2009) 348–352.
[9] C. Comninellis, Electrocatalysis in the electrochemical conversion/combustion of organic pollutants for waste water treatment, Electrochim. Acta 39 (1994) 1857–1862.
[10] B. Correa-Lozano, C. Comninellis, A. De Battisti, Service life of $Ti/SnO_2–Sb_2O_5$ anodes, J. Appl. Electrochem. 27 (1997) 970–974.
[11] J. Iniesta, P.A. Michaud, M. Panizza, G. Cerisola, A. Aldaz, C. Comninellis, Electrochemical oxidation of phenol at boron-doped diamond electrode, Electrochim. Acta 46 (2001) 3573–3578.
[12] F. Montilla, P.A. Michaud, E. Morallon, J.L. Vazquez, C. Comninellis, Electrochemical oxidation of benzoic acid at boron-doped diamond electrodes, Electrochim. Acta 47 (2002) 3509–3513.
[13] A. Kraft, M. Stadelmann, M. Blaschke, Anodic oxidation with doped diamond electrodes: a new advanced oxidation process, J. Hazard. Mater. 103 (2003) 247–261.
[14] M.A. Rodrigo, P.A. Michaud, I. Duo, M. Panizza, G. Cerisola, C. Comninellis, Oxidation of 4-chlorophenol at boron-doped diamond electrode for wastewater treatment, J. Electrochem. Soc. 148 (2001) D60–D64.
[15] E. Brillas, B. Boye, I. Sirés, J.A. Garrido, R.M. Rodriguez, C. Arias, P.L. Cabot, C. Comninellis, Electrochemical destruction of chlorophenoxy herbicides by anodic oxidation and electro-Fenton using a boron-doped diamond electrode, Electrochim. Acta 49 (2004) 4487–4496.
[16] C.A. Martinez-Huitle, E. Brillas, Decontamination of wastewaters containing synthetic organic dyes by electrochemical methods. A general review, Appl. Catal. B 87 (2009) 105–145.
[17] M. Panizza, P.A. Michaud, G. Cerisola, C. Comninellis, Anodic oxidation of 2-naphthol at boron-doped diamond electrodes, J. Electroanal. Chem. 507 (2001) 206–214.
[18] J. Iniesta, P.A. Michaud, M. Panizza, C. Comninellis, Electrochemical oxidation of 3-methylpyridine at a boron-doped diamond electrode: application to electroorganic synthesis and wastewater treatment, Electrochem. Commun. 3 (2001) 346–351.
[19] B. Louhichi, M.F. Ahmadia, N. Bensalah, A. Gadri, M.A. Rodrigo, Electrochemical degradation of an anionic surfactant on boron-doped diamond anodes, J. Hazard. Mater. 158 (2008) 430–437.
[20] A. Giannis, M. Kalaitzakis, E. Diamadopoulos, Electrochemical treatment of olive mill wastewater, J. Chem. Technol. Biotechnol. 82 (2007) 663–671.
[21] W. Gernjak, M.I. Maldonado, S. Malato, J. Caceres, T. Krutzler, A. Glacer, R. Bauer, Pilot-plant treatment of olive mill wastewater (OMW) by solar TiO_2 photocatalysis and solar photo-Fenton, Sol. Energy 77 (2004) 567–572.
[22] HACH, Water Analysis Handbook, second ed., Loveland, Co, USA, HACH Company, 1992.
[23] D. Mantzavinos, E. Lauer, M. Sahibzada, A.G. Livingston, I.S. Metcalfe, Assessment of partial treatment of polyethylene glycol wastewaters by wet air oxidation, Water Res. 34 (2000) 1620–1628.
[24] J.C. Jochimsen, M.R. Jekel, Partial oxidation effects during the combined oxidative and biological treatment of separated streams of tannery wastewater, Water Sci. Technol. 35 (4) (1997) 337–345.
[25] C. Comninellis, C. Pulgarin, Anodic oxidation of phenol for waste water treatment, J. Appl. Electrochem. 21 (1991) 703–708.
[26] P. Canizares, J. Lobato, R. Paz, M.A. Rodrigo, C. Saez, Electrochemical oxidation of phenolic wastes with boron-doped diamond anodes, Water Res. 39 (2005) 2687–2703.
[27] D.C. Montgomery, Design and Analysis of Experiments, fifth ed., John Wiley & Sons, New York, 2001.
[28] A. Deligiorgis, N.P. Xekoukoulotakis, E. Diamadopoulos, D. Mantzavinos, Electrochemical oxidation of table olive-processing wastewater over boron-doped diamond electrodes: treatment optimization by factorial design, Water Res. 42 (2008) 1229–1237.
[29] A. Bedoui, M.F. Ahmadi, N. Bensalah, A. Gadri, Comparative study of Eriochrome black T treatment by BDD-anodic oxidation and Fenton process, Chem. Eng. J. 146 (2009) 98–104.
[30] A.M. Polcaro, A. Vacca, S. Palmas, M. Mascia, Electrochemical treatment of wastewater containing phenolic compounds: oxidation at boron-doped diamond electrodes, J. Appl. Electrochem. 33 (2003) 885–892.
[31] M. Panizza, G. Cerisola, Removal of colour and COD from wastewater containing acid blue 22 by electrochemical oxidation, J. Hazard. Mater. 153 (2008) 83–88.
[32] S. Hammami, A. Ouejhania, N. Bellakhala, M. Dachraoui, Application of Doehlert matrix to determine the optimal conditions of electrochemical treatment of tannery effluents, J. Hazard. Mater. 163 (2009) 251–258.
[33] E. Hamed, A.J. Sakr, Application of multiple response optimization technique to extended release formulations design, Controlled Release 73 (2001) 329–338.
[34] G.E.P. Box, W.G. Hunter, J.S. Hunter, Statistics for Experimenters, John Wiley & Sons, New York, 1978.
[35] M. Panizza, A. Kapalka, C. Comninellis, Oxidation of organic pollutants on BDD anodes using modulated current electrolysis, Electrochim. Acta 53 (2008) 2289–2295.
[36] E. Chatzisymeon, N.P. Xekoukoulotakis, E. Diamadopoulos, A. Katsaounis, D. Mantzavinos, Boron-doped diamond anodic treatment of olive mill wastewaters: statistical analysis, kinetic modelling and biodegradability, Water Res. 43 (2009) 3999–4009.
[37] R.A. Noulty, D.G. Leaist, Diffusion coefficient of aqueous benzoic acid at 25 °C, J. Chem. Eng. Data 32 (1987) 418–420.
[38] E. Chatzisymeon, A. Dimou, D. Mantzavinos, A. Katsaounis, Electrochemical oxidation of model compounds and olive mill wastewater over DSA electrodes. 1. The case of Ti/IrO_2 anode, J. Hazard. Mater. 167 (2009) 268–274.
[39] A.G. Bard, L.R. Faulkner, Electrochemical Methods, Fundamentals and Applications, second ed., John Wiley & Sons, New York, 2001.
[40] M. Panizza, G. Cerisola, Electrochemical degradation of gallic acid on a BDD anode, Chemosphere 77 (2009) 1060–1064.
[41] T. Velegraki, D. Mantzavinos, Conversion of benzoic acid during TiO_2-mediated photocatalytic degradation in water, Chem. Eng. J. 140 (2008) 15–21.
[42] M.I. Pariente, F. Martınez, J.A. Melero, J.A. Botas, T. Velegraki, N.P. Xekoukoulotakis, D. Mantzavinos, Heterogeneous photo-Fenton oxidation of benzoic acid in water: effect of operating conditions, reaction by-products and coupling with biological treatment, Appl. Catal. B 85 (2008) 24–32.

[43] A.H.C. Chan, C.K. Chan, J.P. Barford, J.F. Porter, Solar photocatalytic thin film cascade reactor for treatment of benzoic acid containing wastewater, Water Res. 37 (2003) 1125–1135.
[44] S. Parra, J. Olivero, L. Pacheco, C. Pulgarın, Structural properties and photoreactivity relationships of substituted phenols in TiO_2 suspensions, Appl. Catal. B 43 (2003) 293–301.
[45] M.A. Miranda, F. Galindo, A.M. Amat, A. Arques, Pyrylium salt-photosensitised degradation of phenolic contaminants present in olive oil wastewaters with solar light. Part II. Benzoic acid derivatives, Appl. Catal. B 30 (2001) 437–444.
[46] M. Panizza, G. Cerisola, Critical review: application of diamond electrodes to electrochemical processes, Electrochim. Acta 51 (2005) 191–199.
[47] B. Marselli, J. Garcia-Gomez, P.A. Michaud, M.A. Rodrigo, C. Comninellis, Electrogeneration of hydroxyl radicals on boron-doped diamond electrodes, J. Electrochem. Soc. 150 (2003) D79–D83.